Author/s:
Yong, JKJ;Cui, J;Cho, KL;Stevens, GW;Caruso, F;Kentish, SE

Title:
Surface Engineering of Polypropylene Membranes with Carbonic Anhydrase-Loaded Mesoporous Silica Nanoparticles for Improved Carbon Dioxide Hydration

Date:
2015-06-09

Citation:
Yong, J. K. J., Cui, J., Cho, K. L., Stevens, G. W., Caruso, F. & Kentish, S. E. (2015). Surface Engineering of Polypropylene Membranes with Carbonic Anhydrase-Loaded Mesoporous Silica Nanoparticles for Improved Carbon Dioxide Hydration. Langmuir, 31 (22), pp.6211-6219. https://doi.org/10.1021/acs.langmuir.5b01020.

Persistent Link:
https://hdl.handle.net/11343/123255

# Surface Engineering of Polypropylene Membranes with Carbonic Anhydrase-Loaded Mesoporous Silica Nanoparticles for Improved Carbon Dioxide Hydration

*Joel K. J. Yong,*[†] *Jiwei Cui,*[§] *Kwun Lun Cho,*[†] *Geoff W. Stevens,*[†] *Frank Caruso,*[§] *and Sandra E. Kentish*[†,*]

[†] Department of Chemical and Biomolecular Engineering, The University of Melbourne, Parkville, VIC 3010, Australia

[§] ARC Centre of Excellence in Convergent Bio-Nano Science and Technology, and the Department of Chemical and Biomolecular Engineering, The University of Melbourne, Parkville, Victoria 3010, Australia

Corresponding Author:

sandraek@unimelb.edu.au*

**Abstract**

Carbonic anhydrase (CA) is a native enzyme that facilitates the hydration of carbon dioxide into bicarbonate ions. This study reports the fabrication of thin films of active CA enzyme onto a porous membrane substrate using the layer-by-layer (LbL) assembly. Deposition of multilayer films consisting of polyelectrolytes and CA was monitored by quartz crystal microgravimetry, while the enzymatic activity was assayed according to the rates of *p*-nitrophenylacetate (*p*-NPA) hydrolysis and $CO_2$ hydration. The fabrication of the films onto a nonporous glass substrate showed $CO_2$ hydration rates of 0.52 ± 0.09 μmol $cm^{-2}$ $min^{-1}$ per layer of bovine CA and 2.6 ± 0.7 μmol $cm^{-2}$ $min^{-1}$ per layer of a thermostable microbial CA. The fabrication of a multilayer film containing the microbial CA on a porous polypropylene membrane increased the hydration rate to 5.3 ± 0.8 μmol $cm^{-2}$ $min^{-1}$ per layer of microbial CA. The addition of mesoporous silica nanoparticles as a film layer prior to enzyme adsorption was found to increase the activity on the polypropylene membranes even further to a rate of 19 ± 4 μmol $cm^{-2}$ $min^{-1}$ per layer of microbial CA. The LbL treatment of these membranes increased the mass transfer resistance of the membrane but decreased the likelihood of membrane pore wetting. These results have potential application in the absorption of carbon dioxide from combustion flue gases into aqueous solvents using gas-liquid membrane contactors.

*Keywords*: Layer-by-layer assembly, enzymatic immobilization, carbon dioxide hydration, thin films, mesoporous silica nanoparticles

## Introduction

Carbon dioxide ($CO_2$) emissions into the atmosphere are of great concern because of the environmental impact associated with climate change. The increase in $CO_2$ emissions is mainly derived from human activity and has followed an increasing trend over the past few decades.[1, 2] Hence, it is important to curb the rate of $CO_2$ emissions into the atmosphere through technologies such as carbon capture and sequestration operations.

The hydration of $CO_2$ into $HCO_3^-$ is known to be the rate-limiting step when absorbing carbon dioxide into an aqueous medium.[3] Hydration rates can be accelerated by a naturally occurring enzyme known as carbonic anhydrase (CA).[4] Therefore, efforts have been made to adsorb CA onto surfaces such as polymethylpentene hollow fiber membranes,[5] hydrogels,[6] activated carbon particles,[7] mesoporous silica,[8] gold nanoparticles conjugated with silica[9] and polyurethane films,[10] such that they can be used as immobilized solid-state catalysts in $CO_2$ capture operations.

Polymeric membranes are promising substitutes for absorbing gaseous $CO_2$ into an aqueous solution. In membrane-based $CO_2$ absorption operations, a feed gas containing $CO_2$ is pumped through one side of the membrane, while the other side of the membrane contains the solvent for absorbing the $CO_2$.[11] The membrane is hydrophobic to prevent solvent leakage into the gas stream. Such membrane contactors are readily scalable[11] and are known to produce $CO_2$ streams of high purity even at high $CO_2$ removal rates.[12] The immobilization of CA onto these membranes would further enhance the rate of $CO_2$ absorption into the solvent. However, the CA layer that is immobilized onto the membrane will also add to the mass transfer resistance of $CO_2$ from the gas phase to the gas-liquid interface. It is preferable that the CA film layer be as thin as possible to reduce the mass transfer resistance,[13] which also allows the gas-liquid interface to be closer to the enzyme molecules for better reaction rates.[14]

Layer-by-layer (LbL) assembly is a well-established technique for the preparation of thin multilayered films of oppositely charged polyelectrolytes onto solid planar substrates[15] or particles.[16] The adsorption of proteins, such as immunoglobulin G,[17] glucose oxidase[18] and peroxidase[19] using LbL assembly have been investigated with the aim of developing immunosensors[17] or immobilized catalysts.[20] The construction of CA bilayers with polyethylene imine (PEI) by the LbL technique has also been reported, with a CA loading of 280 ng $cm^{-2}$, as determined by quartz crystal microgravimetry (QCM).[21]

It has been shown that the immobilization of CA onto nanoparticles may further enhance the enzyme activity,[9] as there is a greater degree of freedom for the enzyme to attach

to the curved surfaces of the nanoparticles[22] and hence preserve the active sites.[23] For example, nonporous silica nanoparticles containing adsorbed CA have already been examined for their ability to hydrate $CO_2$.[24] Mesoporous nanoparticles can further increase the enzymatic loading in comparison with nonporous nanoparticles by providing high surface areas with pores that are similar to the size of the target enzyme molecules.[25, 28, 29] Nanosized particles are selected in preference to micron sized particles to reduce the need for intra-particular mass transfer of $CO_2$, as such transport limitations have been shown to cause a reduction in the overall kinetics.[26]

It has been shown that such nanoparticles can be dispersed within a polymer solution prior to casting as a flat sheet membrane, but that these nanoparticles are prone to leaching.[23] Alternatively, submicrometer hollow spheres that are resistant to leaching from aqueous solvents have been fabricated through the LbL technique using alternating layers of silica nanoparticles and polyelectrolytes.[16] Enzymes that are immobilized within such LbL films are known to exhibit enhanced stabilities relative to their free states and can maintain their activity levels within the film for a longer period of time.[27]

Herein, we report the fabrication of CA multilayer films both with and without the addition of mesoporous nanoparticles. We investigate the activity of the resulting films when deposited on both a smooth nonporous planar glass substrate and a commercial hydrophobic polypropylene porous membrane. The CA that was adsorbed within the films was found to increase the rate of $CO_2$ conversion into $HCO_3^-$ ions, with a linear correlation between the number of CA layers adsorbed and the quantity of $CO_2$ converted into $HCO_3^-$. The specific enzyme activity was comparable to that of the free enzyme when it was immobilized within a polyelectrolyte film, but there was a significant decrease in the specific activity upon immobilization within the mesoporous nanoparticles. Enzyme activity also fell somewhat upon incubation at pH 12, typical of the conditions that might be experienced in a carbon capture operation. In addition, the films also provided increased resistance against water penetration into the membrane pores even though they caused the membrane surface to become more hydrophilic.

## Materials and Methods

### Materials Used

Polyethyleneimine (PEI, 25 kDa), polystyrene sulfonate (PSS, 70 kDa), polyallylamine hydrochloride (PAH, 10 kDa), *para*-nitrophenol (*p*-NP), *para*-

nitrophenylacetate (*p*-NPA) and trishydroxymethylaminomethane (Tris) were obtained from Sigma-Aldrich (Castle Hill, NSW, Australia). Concentrated hydrochloric acid (HCl, 37%) and concentrated sulphuric acid ($H_2SO_4$, 98%) were purchased from Scharlau (Gillman, SA, Australia). Compressed $CO_2$ was supplied by Coregas (Thomastown, VIC, Australia). Calcium chloride dihydrate ($CaCl_2 \cdot 2H_2O$), sodium chloride (NaCl), sodium hydroxide (NaOH) and 30% hydrogen peroxide ($H_2O_2$) were obtained from ChemSupply (Gillman, SA, Australia). A suspension of silica particles (50 mg $mL^{-1}$, 2.78 μm diameter) in water was obtained from Microparticles GmbH (Berlin, Germany). All chemicals were used as purchased unless otherwise stated. Ultrapure water was obtained from a Milli-Q purification system (Merck Millipore, Kilsyth, VIC, Australia) with a resistivity of more than 18.2 MΩ cm. Tris buffer (10 mM or 50 mM, pH 6.4 or pH 7.2) was prepared in Milli-Q water and the pH was adjusted by dropwise addition of hydrochloric acid (1 M). The polyelectrolytes (i.e., PEI, PSS, and PAH) solutions were all prepared in Tris buffer (pH 7.2) at a concentration of 1 mg $mL^{-1}$.

Two sources of CA were used. The first source was a commercial form derived from bovine erythrocytes, referred to hereafter as BCA (Sigma-Aldrich product C-3934) and provided in a powder form, with an activity of 2500 Wilbur-Anderson units per mg of protein. BCA with a concentration of 0.2 mg $mL^{-1}$ was prepared in Tris buffer (pH 7.2) prior to use. The second source was an experimental thermostable microbial CA produced by Novozymes A/S (Bagsvaerd, Denmark), referred to hereafter as NCA. The enzyme was produced by microbial fermentation in a benign host organism, which was removed during recovery of the enzyme broth and is not present in the sample. The NCA in the solution had a $CO_2$ hydration activity that was equivalent to 320 g $L^{-1}$ of BCA. The NCA solution was filtered through 0.22 μm syringe filters to remove suspended solids for zeta potential and quartz crystal microgravimetry (QCM) analysis and then diluted with Tris buffer (pH 7.2) to 2% of its original concentration prior to use.

Flat sheet polypropylene (PP) membrane coupons were obtained from Sterlitech Corporation (Kent, WA, USA). These membranes have a pore size of 0.10 μm, a thickness of 75-110 μm and a diameter of 47 mm as per the information provided by the supplier.

Mesoporous silica (MS) nanoparticles with an average size of 110 nm were synthesized according to a previously reported method.[28] These particles were suspended in Tris buffer (pH 7.2) containing 0.1 M NaCl[16] to a particle concentration of 5 mg $mL^{-1}$ and sonicated for 5 min to ensure an even dispersion of the particles prior to layering.

**Zeta-Potential (ζ) Measurements of the Silica Particles**

Approximately 100 μL of the silica particle suspension (50 mg $mL^{-1}$) was mixed with 1 mL of polyelectrolyte solution in Tris buffer for 5 min to deposit a polyelectrolyte layer. The particles were then spun down at 4000 g for 45 s and the supernatant was discarded. The particles were redispersed in 700 μL of Tris buffer (10 mM, pH 7.2) via vortex and were centrifuged at 4000 g to remove free polyelectrolytes.

The washing step was repeated three times to remove all free polyelectrolyte before the deposition of the next polyelectrolyte layer. Approximately 1 μL of the particle suspension was removed after the addition of each polyelectrolyte layer and mixed with 700 μL of Tris buffer (10 mM, pH 7.2) for zeta-potential measurements on a Malvern Zetasizer Nano ZS instrument (Worcestershire, UK). A precursor PEI/$[PSS/PAH]_2$ film was deposited prior to introducing the CA enzyme, which was then either alternately layered with PAH or PSS onto the precursor film.

**Quartz Crystal Microgravimetry**

QCM was used to determine the mass of enzyme adsorbed per unit area on AT cut 5 MHz QCM quartz crystals using a Q-Sense E4 Auto system to quantify the changes in the resonant frequency. Prior to QCM experiments, the crystal surfaces were cleaned with piranha solution (30% $H_2O_2$ mixed with 70% $H_2SO_4$. *Caution! Piranha solution is extremely reactive and corrosive, only small volumes should be prepared freshly for use*) for 5 min, washed with Milli-Q water and ethanol, dried under a stream of nitrogen gas and irradiated with ultraviolet rays for 20 min. The changes in the resonance frequency of the crystals during multilayer deposition were monitored at the third overtone at room temperature. Three layers of CA were deposited for each crystal.

Deposition steps and washing steps were conducted for 3 min and 2 min, respectively, with 250 μL aliquots of polyelectrolyte solution or Milli-Q water at a flow rate of 0.579 mL $min^{-1}$. After the formation of a PEI/$[PSS/PAH]_2$ precursor film showing regular stepwise film growth,[29] CA was deposited onto the quartz crystals sequentially with the polyelectrolytes to form multilayer enzyme films. QCM was also used to investigate the construction of NCA films in a similar manner.

The Sauerbrey equation was used to determine the mass of material deposited onto the quartz crystal, which had an active area of 1 cm in diameter. This equation is valid when the ratio of the change in the dissipation factor ΔD is less than $10^{-7}$ times per change of Hz in

the resonant frequency (ΔF).[30] The change in ΔF of the quartz crystals is linearly dependent on the mass of material (Δm) deposited onto the crystal:

$$\Delta F = -\frac{n\Delta m}{C} \qquad Equation\ 1$$

where n is the number of overtones and C is a constant (17.7 ng $Hz^{-1}$ $cm^{-2}$ for a 5 MHz AT cut crystal from Q-Sense). Equation 1 can be rewritten to relate the layer thickness (*x*) to the change in the observed resonant frequency of the crystal (ΔF) and the density of the film (ρ):[29]

$$x = -(2.12 \times 10^{-4})\frac{\Delta F}{\rho} \qquad Equation\ 2$$

The surface area of the crystal can be estimated to be approximately 20% larger after enzyme deposition.[20] The densities of protein and polyelectrolyte layers have been previously assumed to be approximately 1.3 ± 0.1 g $cm^{-3}$ and 1.2 ± 0.1 g $cm^{-3}$, respectively.[20] For estimating the *maximum* theoretical film thickness of the hybrid polyelectrolyte/protein film, a film density of 1.2 ± 0.1 g $cm^{-3}$ was assumed.

**Enzyme Adsorption onto Smooth, Non-Porous Surfaces**

Glass slides (22 mm × 22 mm) were treated with piranha solution, Milli-Q water and ethanol in the same way as the QCM crystals prior to adsorption experiments. A PEI/$[PSS/PAH]_2$ precursor film was first deposited by immersing the glass slides or the silicon wafers into the respective polyelectrolyte solutions for 5 min. After the deposition of each layer, excess polyelectrolyte was removed by rinsing with excess Tris buffer (pH 7.2).

BCA or NCA was then adsorbed onto microscopic glass slides to form multilayered enzyme films similar to the films that were prepared on the QCM crystals. Both sides of the glass slides were exposed to the polyelectrolyte solutions.

**Enzyme Immobilization onto Flat Sheet Membranes**

PP membrane coupons were placed onto a glass substrate. Polyelectrolyte solutions were coated onto the active side of the membrane surface using a commercial paintbrush (Woolworths Ltd, Bella Vista, New South Wales, Australia) to spread the solution evenly across the membrane. Each polyelectrolyte solution was left on the surface of the membranes for 3 min before rinsing with excess Tris buffer (pH 7.2).

**Enzyme Immobilization with MS Nanoparticles**

To investigate the effect of the MS nanoparticles on the adsorption and the activity of the NCA, fresh glass slides or membrane coupons were coated sequentially as $[MS/NCA/PAH]_2/MS/NCA$ after the deposition of the precursor film. The membranes were contacted with the MS particles or the NCA solution for 20 min before washing with buffer and then contacted with PAH for 5 min before washing with buffer. The film that was formed is denoted as the MSNCA film. The quantity of enzyme that was adsorbed was determined by analyzing the supernatant using UV-Vis spectrophotometry on a Varian Cary 1E UV-Vis spectrophotometer (Agilent Technologies, Mulgrave, VIC, Australia) with 10 mm quartz cuvettes (Starna Pty Ltd, Baulkham Hills, NSW, Australia) at a wavelength of 280 nm.

**Electron Microscopy**

The MS nanoparticles were imaged by transmission electron microscopy (TEM) using a FEI Tecnai TF20 microscope at a voltage of 200 kV after being placed onto Formvar-coated copper grids and dried in air.

The glass slides and the membrane coupons containing adsorbed enzyme were dried under a nitrogen stream, gold sputter-coated and analyzed using a Phillips XL30 FEG field emission scanning electron microscope (FESEM) at a voltage of 2.0 kV to determine the surface morphologies of the glass slides before and after protein adsorption. A wetted membrane coupon containing the adsorbed MS nanoparticles was immersed in liquid nitrogen for 5 min and then fractured for an analysis of the membrane cross-section.

**Characterization of the Flat Sheet Membranes**

The liquid entry pressure (LEP) of the membranes was measured by placing a membrane coupon of 4.8 cm in diameter within a dead-end filtration cell (Sterlitech HP4750, Kent, WA, USA) that had an active filtration area of 3.2 cm in diameter. The cell was pressurized with air and increased in 50 kPa steps every 5 min to determine the pressure that was sufficient to force water through the membrane. Water flux tests were then conducted for the different membranes at a constant pressure (greater than the LEP) to determine the permeability of the membrane. The membranes were then air dried after the water flux tests for 72 h. Contact angle measurements were performed on the dry membranes using a FTÅ200 dynamic contact angle analyzer (First Ten Ångstroms, Portsmouth, VA, USA).

**Characterization of Enzyme Activity**

The enzymatic activity of the adsorbed BCA on the glass slides was initially determined based on the rate that the adsorbed BCA converted *p*-NPA to *p*-NP. Solutions of *p*-NPA in acetonitrile (2.5 mg $mL^{-1}$) were mixed with Tris buffer (pH 7.2) at a volumetric ratio of 1:9 for the activity assays.[10, 31] CA-coated glass slides were incubated within a 20 mL aliquot of *p*-NPA solution, and a small volume of the mixture was extracted at set timepoints and analyzed by UV-Vis spectrophotometry at 348 nm to determine the total concentration of *p*-NP and *p*-nitrophenoxide in solution[32] for calculating the rate of *p*-NPA hydrolysis.

The activity of the immobilized enzymes on the glass slides and the membranes were also quantified for their ability to hydrate $CO_2$ into $HCO_3^-$, based on the method provided by Vinoba and co-workers.[8, 9] A saturated $CO_2$ solution was prepared by passing a $CO_2$ gas stream into a bottle of Milli-Q water at 25°C for 1 h. Approximately 40 mL of Tris buffer (pH 6.4) was added to 100 mL of the saturated $CO_2$ solution before the enzyme-coated glass slide or the membrane coupon was immersed into the mixture. The mixture was stirred for 1 min followed by the removal of the glass slide or the membrane coupon before the addition of 20 mL of $CaCl_2 \cdot 2H_2O$ solution (5.3% w/v) and 10 mL of NaOH solution (1 M) to quench the reaction and precipitate the $Ca(HCO_3)_2$ as $CaCO_3$. The precipitated $CaCO_3$ was then filtered, dried in an oven at 80°C overnight and weighed to determine the quantity of $CO_2$ that had been hydrated based on the quantity of $CaCO_3$ produced.

A separate activity test was set up for the determination of the free NCA activity in solution. A sample of 2% NCA in Tris buffer (pH 7.2) was sequentially diluted to various levels of dilution, and 1 mL aliquots of diluted NCA was added to different batches of 100 mL saturated $CO_2$ solution and stirred for 1 min before adding 20 mL of $CaCl_2 \cdot 2H_2O$ solution (5.3% w/v) and 10 mL of NaOH solution (1 M) to quench the reaction. The precipitated $CaCO_3$ was then filtered and dried before determining the quantity of $CaCO_3$ that was produced.

Control experiments were conducted to determine the quantity of $CaCO_3$ that was produced in the absence of any enzyme. Any incremental $CaCO_3$ that was produced in the presence of CA was then attributed to the hydration activity of the enzyme.

Free NCA samples and membrane samples containing adsorbed NCA were also directly compared for their pH stability via incubation either in a 0.2 M KCl solution (adjusted to pH 12 with NaOH) or in Tris buffer (pH 7.2) for 72 h at 4°C. This stability is important as most carbon dioxide absorption systems operate at pH greater than 10.

## Results and Discussion

### Enzyme Adsorption and Multilayer Film Formation

Zeta-potential measurements of PAH/CA and PSS/CA layers deposited onto silica spheres at pH 7.2 confirmed that both BCA and NCA are negatively charged (Figure 1). However, the inability of either enzyme to reverse the surface zeta potential when applied after the positively charged PAH layer indicates that these proteins possess only a weak net negative charge at the measurement pH of 7.2. This weak net negative charge is consistent with the reported isoelectric points for commercial BCA, which range from pH 4.9 to pH 6.7.[33]

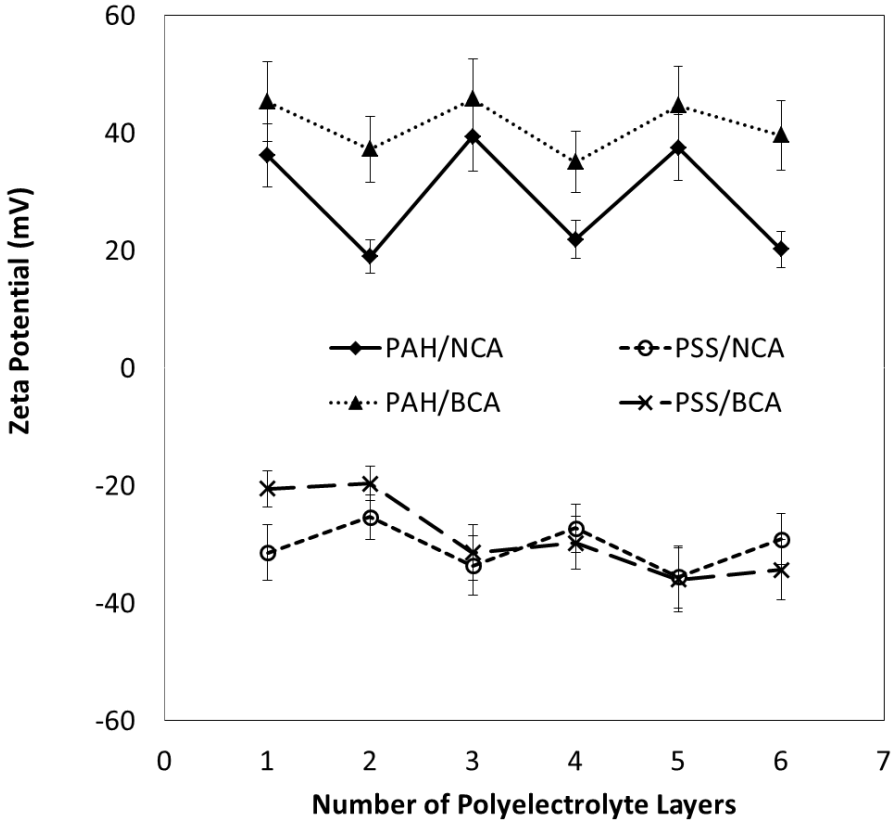


**Figure 1**. Zeta-potential measurements for PAH/BCA, PSS/BCA, PAH/NCA and PSS/NCA bilayers prepared in a Tris buffer solution at pH 7.2. The odd numbered layers (1, 3 and 5) represent PAH or PSS layers, while the even numbered layers (2, 4 and 6) represent BCA or NCA layers.

The lack of surface charge inversion prevents the uniform addition of extra PSS/CA or PAH/CA bilayers sequentially beyond the first bilayer, as stepwise growth in multilayer film formation requires a complete reversal in the surface charge.[29] This is demonstrated by the limiting changes in zeta-potential for successive PSS/CA and PAH/CA bilayers in Figure 1.

Consistent with these data, QCM investigations showed that CA was readily adsorbed onto PAH or PSS, but the subsequent deposition of PAH onto a PAH/CA film or PSS onto a PSS/CA film resulted in no further mass being added onto the quartz crystal, similar to what was observed elsewhere for an invertase/poly(dimethyldiallylammonium chloride) system.[34]

CA films were also prepared on a QCM crystal to determine the adsorption of BCA onto alternating PAH and PSS layers, as a BCA/PSS/BCA/PAH/BCA film (Figure 2a) and a PSS/BCA/PAH/BCA/PSS/BCA film (Figure 2b). However, for both cases, the rate of decrease in frequency slowed after repeated depositions of CA, which was again consistent with the ζ-potential results. The quantity of BCA deposited onto PAH layers was greater than that deposited onto PSS layers, reflecting the stronger electrostatic attraction forces between the negatively charged BCA and the positively charged PAH. The $\Delta D$:$\Delta F$ ratios were consistently of the order $10^{-8}$ $Hz^{-1}$, which reflects that Equation 1 is valid for estimating the mass of polyelectrolyte being deposited onto the quartz crystal surface.

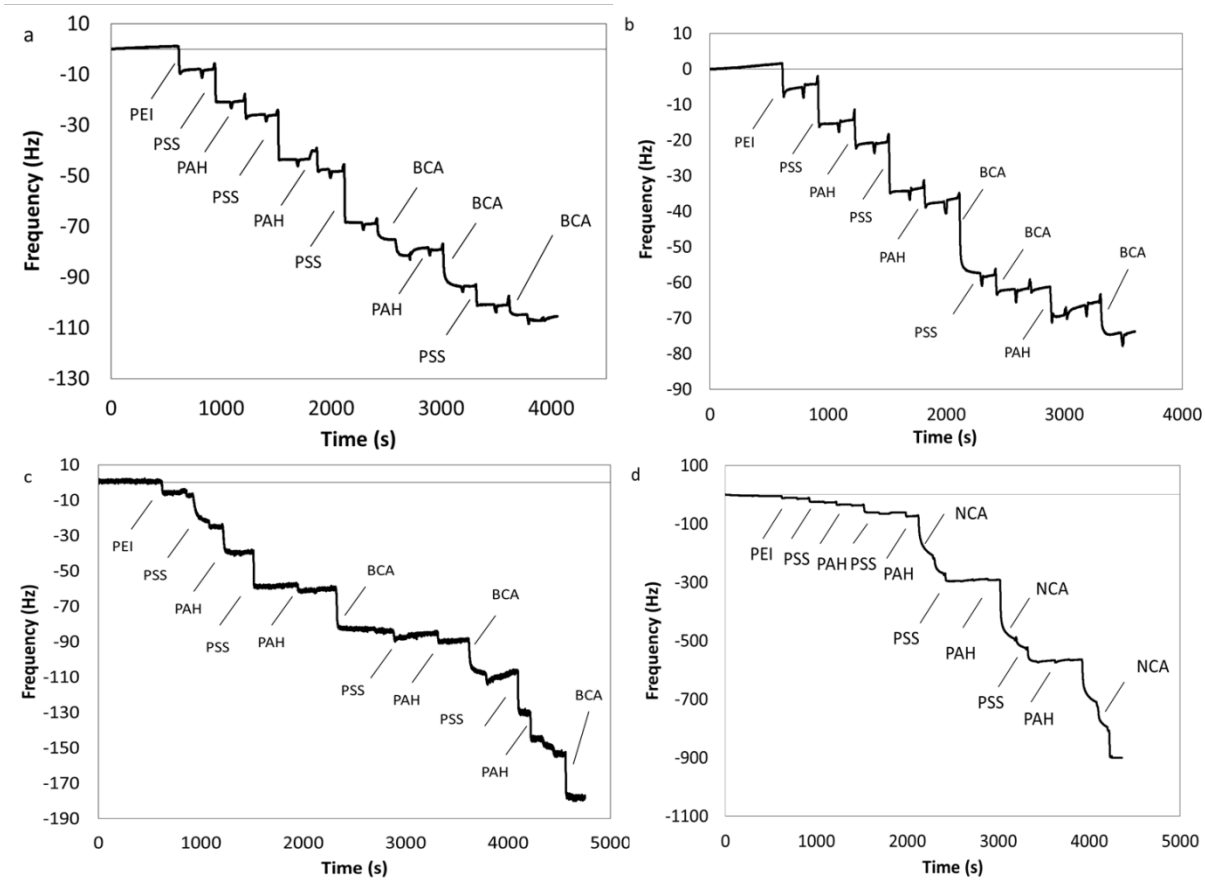


**Figure 2**. Real-time QCM investigations of the deposition of (a) PSS/BCA/PAH/BCA/PSS/BCA, (b) PAH/BCA/PSS/BCA/PAH/BCA, (c) $[BCA/PSS/PAH]_2/BCA$, and (d) $[NCA/PSS/PAH]_2/NCA$ multilayers.

However, the deposition of BCA/PSS/PAH (Figure 2c) or NCA/PSS/PAH (Figure 2d) in repeating trilayers gave a better indication of consistent film formation in comparison to the films that were fabricated in Figures 2a or 2b. A frequency decrease of 226 ± 11 Hz per layer of NCA was observed for a $[NCA/PSS/PAH]_2$/NCA film (Figure 2d), which translates into an NCA coverage of 790 ± 30 ng $cm^{-2}$. This value is significantly greater than the single layer enzyme loading obtained from a covalent coupling of the same enzyme to a surface (less than 100 ng $cm^{-2}$).[7, 35] This value was also higher than the 280 ng $cm^{-2}$ of CA that was deposited as PEI/CA bilayers in prior work (the type of CA that was used was unspecified).[21]

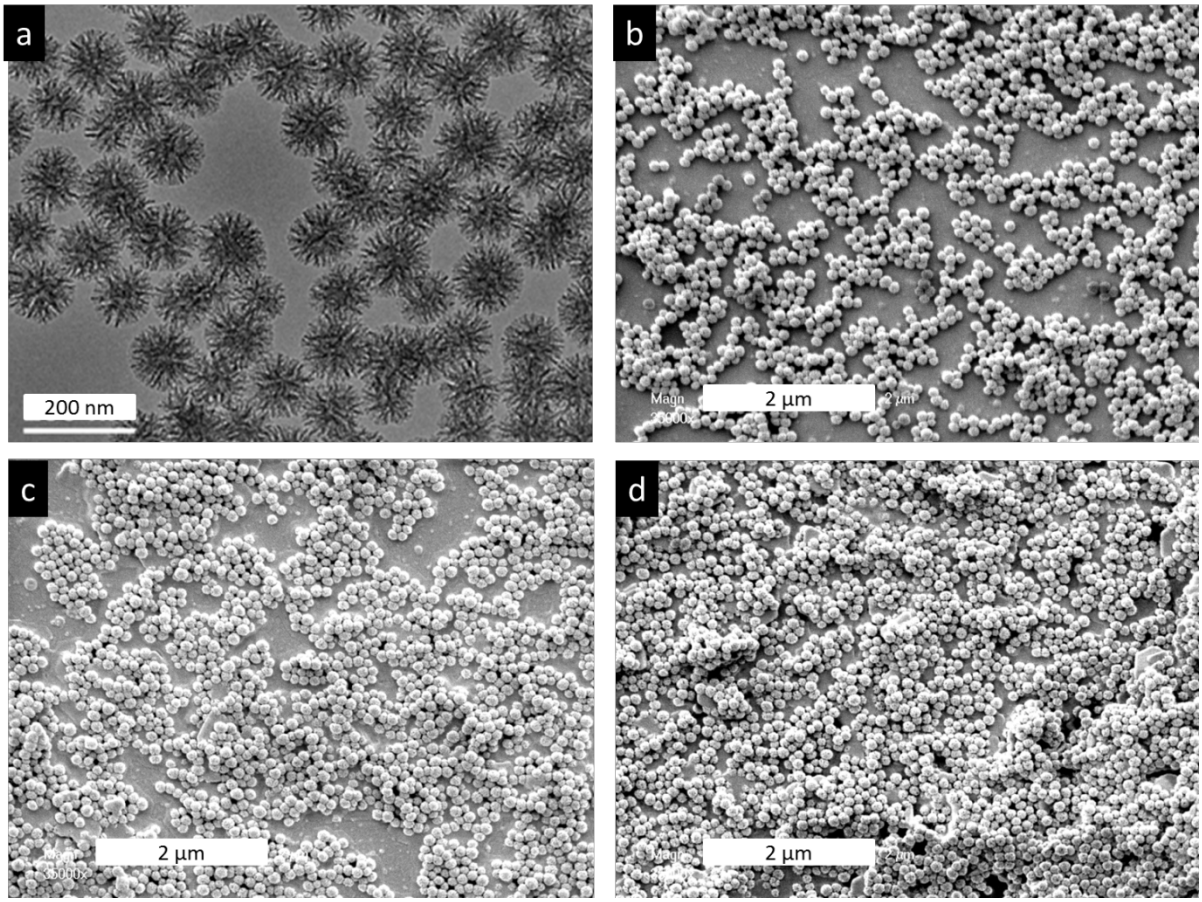


**Figure 3**. (a) TEM image of the MS nanoparticles before deposition. SEM images of MS nanoparticles on silicon wafers after (b) one layer, (c) two layers, (d) three layers of coating. Scale bars in (b-d) are 2 µm.

To increase the quantity of enzyme being immobilized onto the films, MS particles with an average size of 115 nm (Figure 3a) were synthesized and used to load NCA in films of $[MS/NCA/PAH]_2$/MS/NCA onto either a glass plate or a silicon wafer (Figures 3 b, c, d). The quantity of NCA adsorbed in this case was determined from the difference in the UV absorbance of the NCA solution before and after contact with the glass substrate. Each coating

of NCA was found to add 190 ± 20 μg $cm^{-2}$ of NCA to the MS layer on the film (Figure 4), which is approximately 140 times greater than the adsorption of NCA onto PAH.

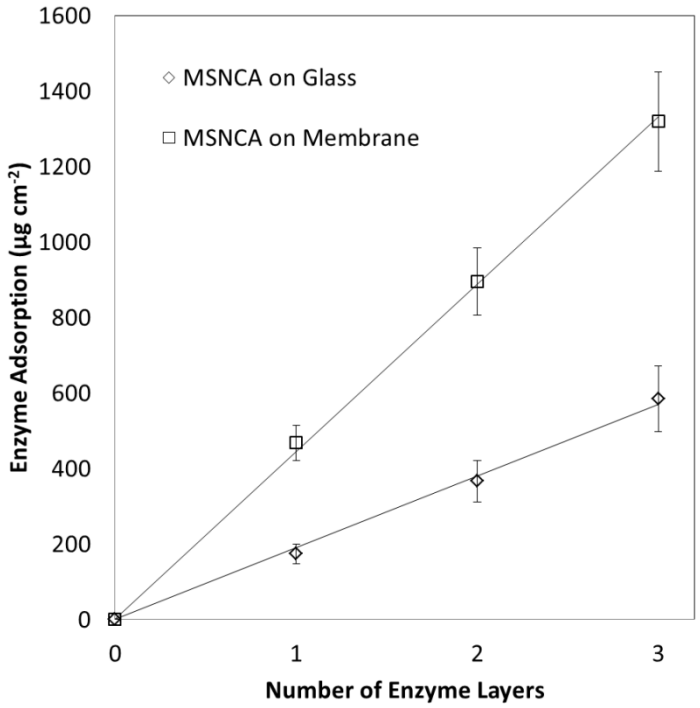


**Figure 4**. Quantity of NCA adsorbed onto each MS nanoparticle layer deposited onto the film.

These significantly increased enzyme loadings are indicative of the mesoporous nanoparticles with their high surface areas allowing for large polymer/protein loadings.[25] In comparison, the concentration of NCA in the supernatant did not change significantly during the fabrication of the $[NCA/PSS/PAH]_2NCA$ film, which is consistent with the lower quantities of enzyme adsorbed onto PAH as compared to the MS nanoparticles.

**Multilayer Film Characterization**

The total thickness of the multilayered protein films can significantly influence the mass transfer performance in membrane contactor applications. Ideally, the deposited polyelectrolyte layers will cover the pores of the top surface (typically 100 nm in diameter) to reduce pore wetting, but their thickness should not result in a significant resistance to the flow of carbon dioxide across the membrane. The total film thickness of the three enzyme layers in addition to the precursor film can be calculated based on Equation 2. These film thicknesses are shown in Table 1:

**Table 1**. Maximum Polyelectrolyte Film Thicknesses

| Polyelectrolyte Film | Maximum Film Thickness (nm) |
|---|---|
| PSS/BCA/PAH/BCA/PSS/BCA[a] | 19 ± 1 |
| BCA/PSS/BCA/PAH/BCA[a] | 14 ± 1 |
| $[BCA/PSS/PAH]_2/BCA$[a] | 38 ± 4 |
| $[NCA/PSS/PAH]_2/NCA$[a] | 154 ± 8 |
| $[MS/NCA/PAH]_2/MS/NCA$[b] | 337 ± 67 |

[a]These results were obtained from QCM measurements. [b]This result was obtained from a cross-sectional SEM analysis of a fractured silicon wafer.

The thickness of the PSS/BCA/PAH/BCA/PSS/BCA and the BCA/PSS/BCA/PAH/BCA films are similar to the protein bilayer thicknesses and the PAH/PSS bilayer thicknesses that have been described elsewhere.[21, 29] The $[BCA/PSS/PAH]_2/BCA$ films were two to three times thicker than the PSS/BCA/PAH/BCA/PSS/BCA or the BCA/PSS/BCA/PAH/BCA films, which can be attributed to more BCA adsorbing onto a PAH precursor layer than onto a PSS precursor layer, as evidenced in the QCM analyses from Figure 2. The average frequency change was 9.2 ± 2.5 Hz when BCA was adsorbed onto PSS, which is approximately half of the 17 ± 5 Hz exhibited by the adsorption of BCA onto PAH.

The thickness of the $[NCA/PSS/PAH]_2/NCA$ films was four times greater than the equivalent thickness of the $[BCA/PSS/PAH]_2/BCA$ films. This reflects the greater mass of NCA and other proteins that adsorb onto the quartz crystal at every deposition step (Figure 2). The $[MS/NCA/PAH]_2/MS/NCA$ film is thicker again as a result of the addition of the MS nanoparticles, which are approximately 115 nm in diameter. A film thickness of approximately 337 ± 67 nm indicates that there is multilayer coverage of the nanoparticles on the surface of the silicon wafer.

**Enzyme Activity Assays**

Within experimental error, the resulting $[BCA/PSS/PAH]_2/BCA$ films exhibited a uniform *p*-NP production rate of 0.10 ± 0.01 μmol $min^{-1}$ $cm^{-2}$. This *p*-NP production rate was irrespective of the number of BCA layers that were adsorbed (Figure 5). However, the PSS/BCA/PAH/BCA/PSS/BCA and the BCA/PSS/BCA/PAH/BCA films showed that the BCA adsorbed preferentially more onto PAH than PSS. The similar *p*-NPA hydrolysis rates (instead of an increased enzymatic activity upon the deposition of more enzyme layers[19])

suggest that the hydrophilic PAH and PSS layers were sufficiently non-porous to limit the diffusion of the large hydrophobic *p*-NPA molecules to the lower layers of immobilized BCA.

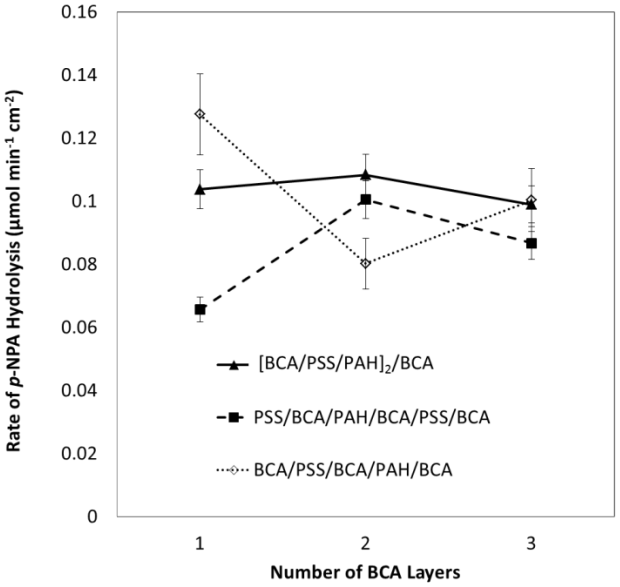


**Figure 5**. Enzymatic activity of $[BCA/PSS/PAH]_2/BCA$, PSS/BCA/PAH/BCA/PSS/BCA and BCA/PSS/BCA/PAH/BCA films in the hydrolysis of *p*-NPA.

However, $CO_2$ is a small uncharged molecule that will be able to penetrate the polyelectrolyte multilayers more readily. Thus, it is necessary to evaluate the contribution of each immobilized CA layer to the overall total enzymatic activity using $CO_2$ hydration assays. Glass slides were prepared with up to three adsorbed layers of CA as $[CA/PSS/PAH]_2/CA$ films and assayed for their $CO_2$ hydration activities.

A calibration curve was first prepared for determining the $CO_2$ hydration activity of the free NCA in a saturated $CO_2$ solution. The activity of the free NCA is shown to be approximately 2.7 μmol $min^{-1}$ $\mu g^{-1}$ of NCA (Figure 6). However, the specific activity of the NCA decreased to 2.1 μmol $min^{-1}$ $\mu g^{-1}$ after it was stored at pH 12 over a period of 72 h at 4°C (Figure 6). A number of other researchers have also shown that CA loses activity upon exposure to high pH.[1, 24] However, the residual activity recorded here (78%) is significantly greater than that observed in this earlier work. Sharma and Bhattacharya[1] observe residual activities of between 24 and 57% across four CA varieties after exposure for only 6 h at pH 10, presumably at ambient temperature. Similarly, Zhang *et al.*[24] observe a residual activity of 63% for a commercial enzyme when tested at pH 10.5 and 4°C.

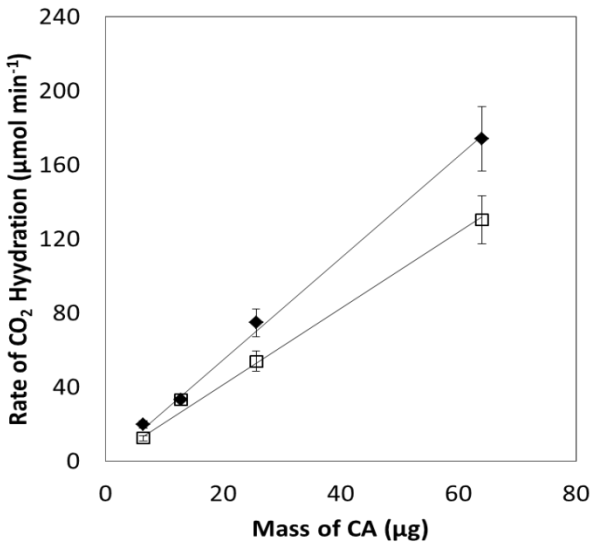


**Figure 6.** $CO_2$ hydration rate as a function of the quantity of free NCA added to solution. The filled diamond symbols (♦) indicate the rate for fresh NCA solution, while the open squares(□) indicate the rate of hydration for NCA that was incubated for 72 hours at pH 12 and 4°C.

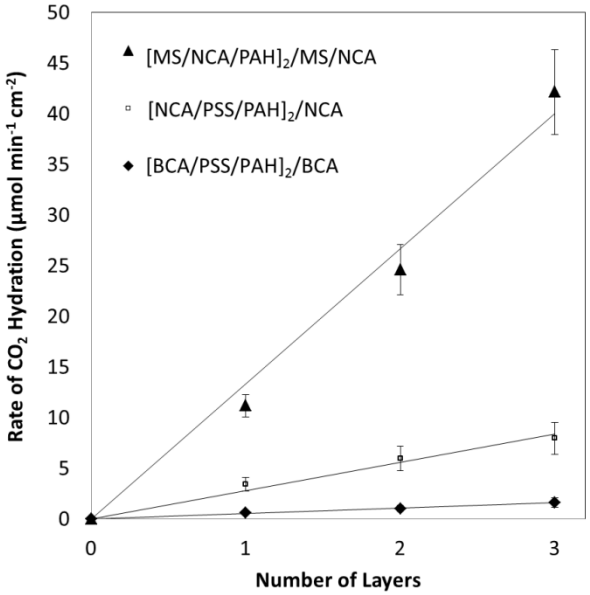


**Figure 7**. $CO_2$ hydration activity as a function of the number of CA layers on glass.

Figure 7 shows that the overall $CO_2$ hydration activity of the [BCA/PSS/PAH]$_2$/BCA film was approximately 0.52 ± 0.09 µmol $min^{-1}$ $cm^{-2}$ per layer of adsorbed BCA. This $CO_2$ hydration activity is approximately 5 times greater than the *p*-NPA hydrolysis activity, which is consistent with the $CO_2$ hydration to *p*-NPA hydrolysis activity ratios that have been reported elsewhere.[32] This activity ratio reflects the limitations of the *p*-NPA diffusion within the film. Moreover, in contrast with the *p*-NPA analyses, the CA activity increases linearly

with the deposition of further layers when hydrating $CO_2$, regardless of the type of CA that was used (Figure 7). This linear trend indicates that the dissolved $CO_2$ is able to readily penetrate through the PAH/PSS bilayers to the lower levels of the film for reaction. It is probable that the activity eventually plateaus with increasing CA layers because of diffusion rate limitations, as was observed in activity assays of immobilized peroxidase enzymes.[19]

The $CO_2$ hydration activity of the film prepared with NCA was observed to be 2.6 ± 0.7 μmol $min^{-1}$ $cm^{-2}$ per layer of adsorbed NCA, which was approximately 5 times greater than that of the BCA film. The specific activity of the NCA in terms of the mass of adsorbed NCA was 3.5 μmol $min^{-1}$ $\mu g^{-1}$, which is comparable within experimental error to the specific activity of the free NCA at 2.7 μmol $min^{-1}$ $\mu g^{-1}$. This indicates that there is no significant loss of activity upon immobilisation onto the plate.

The addition of the MS nanoparticles onto the glass plate further boosts the $CO_2$ hydration activity to 13 ± 4 μmol $min^{-1}$ $cm^{-2}$ per layer of adsorbed NCA. However, given that the adsorption of NCA was as high as 190 μg $cm^{-2}$ NCA (Figure 4), this $CO_2$ hydration activity translates to a specific NCA activity of 0.067 μmol $min^{-1}$ $\mu g^{-1}$. This specific activity is a decrease of 97.5% in comparison with the specific activity of the free enzyme at 2.7 μmol $min^{-1}$ $\mu g^{-1}$ NCA. Therefore, there is a loss of enzymatic activity when the NCA is immobilized onto the nanoparticles, which was not observed for immobilization upon the glass plate. Similar losses in enzymatic activity have been reported previously for both nonporous nanoparticles[24] and porous nanoparticles.[39] In the present case, the decline in the specific enzyme activity is likely to be the result of the added diffusional resistance for the $CO_2$ molecules[39] when entering the pores of the MS nanoparticles.

**Membrane Characterization**

When coated on the surface of a porous polypropylene membrane, the MS particles continue to outperform a simple multilayer film, in this case by a factor of four (Figure 8) at an average rate of 19 ± 4 μmol $cm^{-2}$ $min^{-1}$ per layer in comparison with the multilayer film performance at 5.3 ± 0.8 μmol $cm^{-2}$ $min^{-1}$ per layer. The enzymatic activity on the membrane is approximately double that of the activity on the flat glass plate (Figure 7). This increased enzymatic activity is consistent with the data in Figure 4, which also shows a doubling in NCA adsorption from 190 to 440 μg $cm^{-2}$ when the plate is replaced with a membrane. This increase in enzyme activity probably reflects some penetration of the enzyme layers into the porous structure.

These hydration rates compare well to the flux rates determined for $CO_2$ absorption within membrane contactors described in the literature. The flux rates for the absorption of $CO_2$ into monoethanolamine through a porous PP contactor range from 1.5 to 30 μmol $cm^{-2}$ $min^{-1}$.[40, 41] The $CO_2$ flux is generally lower for solvents with slower reaction kinetics such as potassium carbonate, where promotion with CA would be of value. Capannelli *et al.*[42] report a flux of approximately 4 μmol $cm^{-2}$ $min^{-1}$ for a 1 M $K_2CO_3$ solution, versus 50 μmol $cm^{-2}$ $min^{-1}$ for the same concentration of piperazine and 30 μmol $cm^{-2}$ $min^{-1}$ for monoethanolamine.

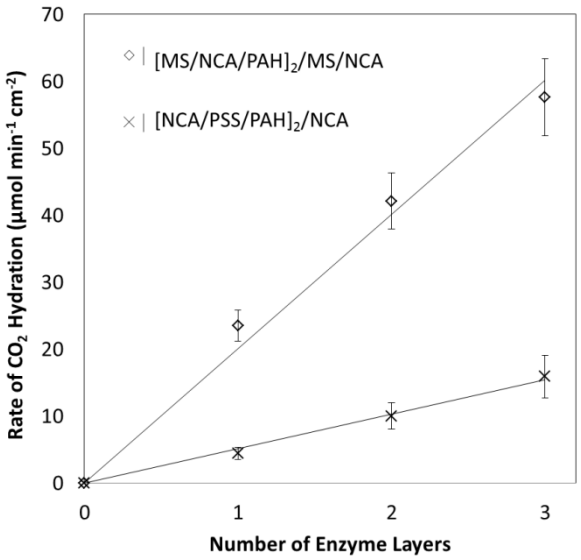


**Figure 8**. $CO_2$ hydration activity as a function of the number of NCA layers on the PP membranes.

Incubation of the membrane films for 72 h at pH 12 leads to a loss of activity, but 70 to 80% of the residual activity is retained, relative to films incubated in Tris Buffer at pH 7.2 for the same period (Figure 9). This is consistent with the data recorded for the free enzyme (Figure 6), indicating that the enzyme is more tolerant of high pH conditions than other strains that have been presented in the literature.[1, 24]

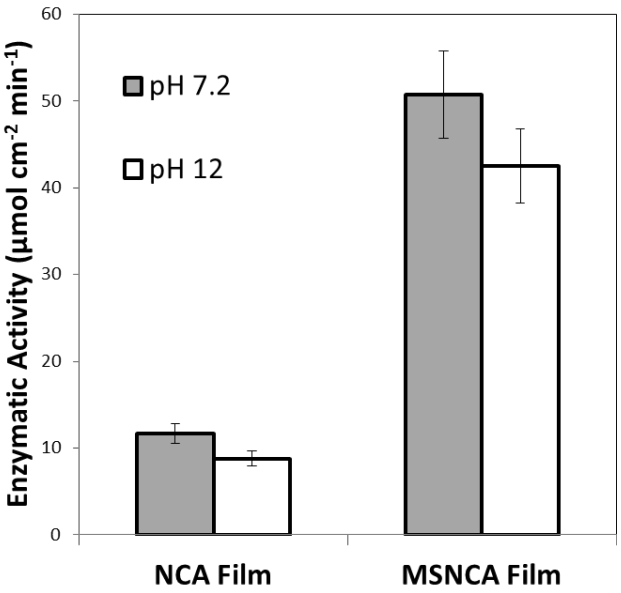


**Figure 9.** The enzymatic activity of the immobilized membrane films both after incubation for 72h at pH 7.2 (grey bars) and at pH 12 (white bars) at 4°C. These films were prepared as $[NCA/PSS/PAH]_2NCA$ films (denoted as NCA) and $[MS/NCA/PAH]_2MS/NCA$ (denoted as MSNCA), respectively.

SEM images of the PP membrane surfaces and cross sections before and after LbL treatment (Figure 10) show clear evidence of the multilayer films and MS spheres on the surface. Figure 10b shows that the $[NCA/PSS/PAH]_2NCA$ layers form a flat dense film[43] that is akin to the formation of nanofiltration-type barriers caused by the interactions between PAH and PSS.[44] Figures 10c and 10d also show that the MS spheres assemble uniformly onto the membrane surface. However, there is little evidence of deep penetration into the porous substructure. (Figures 10e and 10f). The multilayer film thicknesses on the membrane surface are of the order of 300-500 nm, consistent with that observed for the flat plate (Table 1). This means that the mass transfer resistance through the membrane itself should not be significantly compromised.

Figure 10d indicates that there has been little degradation of the MS spheres after storage at pH 12 for 72 h. However, it should be noted that silica materials will dissolve in an alkaline environment over a long period of time. The instability of silica materials at high pH could limit the use of the MS nanoparticles in carbon capture applications operating under high pH conditions.

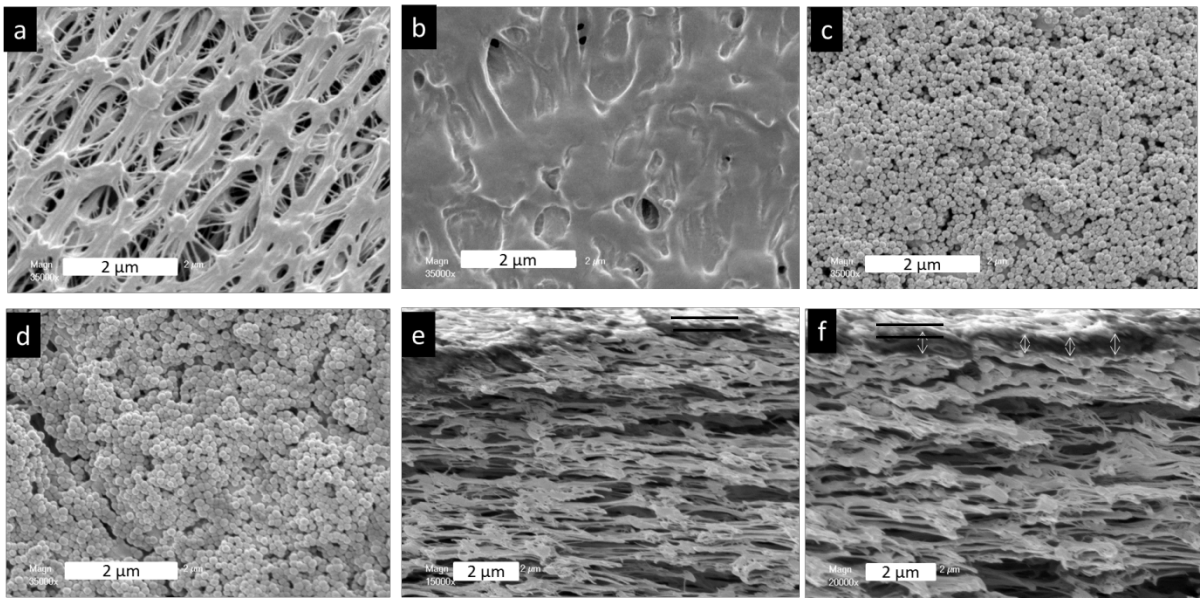


**Figure 10**. The PP membrane surface (a) before LbL treatment, (b) after LbL treatment with $[NCA/PSS/PAH]_2NCA$, (c) after LbL treatment with $[MS/NCA/PAH]_2MS/NCA$ and storage at pH 7.2 for 72 h, (d) after LbL treatment with $[MS/NCA/PAH]_2MS/NCA$ and storage at pH 12 for 72 h. The PP membrane cross-section (e) after LbL treatment with $[NCA/PSS/PAH]_2NCA$, (f) after LbL treatment with $[MS/NCA/PAH]_2MS/NCA$. The black bars in (e) and (f) indicate the approximate thickness of the LBL films.

It is well known that the pores of the membrane must remain filled with gas to maintain effective mass transfer rates in a membrane contactor,[45] and a reduction of the local pore diameter could assist in preventing the wetting of the pore volume with solvent.[46, 47] Conversely, the deposition of CA and other polyelectrolytes on the membrane surface could reduce the contact angle and so enhance wetting. In the present case, the pressure required to force water through the membrane (the liquid entry pressure) was recorded experimentally, as an indication of these competing effects (Table 2):

***Table 2***. Characterization of the PP membrane before and after LbL treatment

| Membrane | Contact Angle (°) | Liquid Entry Pressure (kPa) | Water Flux (kg $m^{-2}$ $h^{-1}$) at 575 kPa |
|---|---|---|---|
| PP (clean) | 96 ± 2 | < 525 | 9.4 ± 0.6 |
| PP (LbL with NCA) | 60 ± 2 | < 550 | 2.25 ± 0.08 |
| PP (LbL with MSNCA) | 52 ± 1 | < 575 | 0.53 ± 0.02 |

Table 2 indicates that the LbL treatment caused the membrane surface to become more hydrophilic, as evidenced by the contact angle measurements. However, an increased pressure was required to force water through the thin film that was fabricated on the membrane, and the water flux was also observed to decline, particularly after LbL treatment with the MSNCA film. This confirms that the average pore size has been reduced significantly, as is evident from the images in Figure 9. The tighter pore size will reduce pore

wetting, but may also increase the resistance to the mass transfer of carbon dioxide across the membrane. A compromise between these two competing effects will be required.

## Conclusions

This work has shown that carbonic anhydrase can be readily applied to the surface of a porous polymeric membrane as a uniform thin film. The use of LbL techniques leads to enzyme loadings that are significantly greater than those previously obtained using covalent coupling. The diffusion of $CO_2$ through these multilayers was unhindered, as evidenced by the uniform increase in $CO_2$ hydration activity with each successive CA layer. The use of a thermostable microbial enzyme (NCA) leads to higher loadings and to greater enzymatic efficiency. The addition of MS nanoparticles to the polyelectrolyte film prior to enzyme adsorption increases the $CO_2$ hydration rates by eightfold relative to the bovine enzyme film. However, the specific activity of the NCA decreased sharply upon immobilization onto the MS nanoparticles, which may be indicative of diffusional resistances for $CO_2$ molecules entering the pores of the nanoparticles for reaction.

While it can be observed that the overall $CO_2$ hydration rates increased when the enzyme was adsorbed onto a membrane, the flux through the membrane declined, which may lead to additional mass transfer resistance in a full scale membrane module. These results show potential towards the development of new membrane materials for use as membrane contactors in $CO_2$ absorption processes. However, the activity of these membranes was only quantified in a stirred solution pre-saturated with carbon dioxide, where mass transfer limitations are avoided. The results need to be validated by work at a larger scale in a gas-liquid membrane contactor format at realistic pH levels and over a longer period of time. This is the focus of our ongoing work.

## Acknowledgements

The work was supported by the Australian Research Council Centre of Excellence in Convergent Bio-Nano Science and Technology (Project number CE140100036) and the Particulate Fluids Processing Centre (PFPC), a Special Research Centre of the Australian Research Council. KLC is the recipient of a John Stocker Postdoctoral Fellowship from the Science and Industry Endowment Fund. Novozymes A/S kindly supplied the enzyme, NCA. These sources of support are gratefully acknowledged.

## References


1. Sharma, A.; Bhattacharya, A., Enhanced Biomimetic Sequestration of $CO_2$ into $CaCO_3$ using Purified Carbonic Anhydrase from Indigenous Bacterial Strains. *J. Mol. Catal. B* **2010,** *67*, 122-128.
2. Samanta, A.; Zhao, A.; Shimizu, G. K. H.; Sarkar, P.; Gupta, R., Post-Combustion $CO_2$ Capture Using Solid Sorbents: A Review. *Ind. Eng. Chem. Res.* **2012,** *2012*, 1438-1463.
3. Yong, J. K. J.; Stevens, G. W.; Caruso, F.; Kentish, S. E., The Use of Carbonic Anhydrase to Accelerate Carbon Dioxide Capture Processes. *J. Chem. Technol. Biotechnol.* **2015,** *90*, 3-10.
4. Shekh, A. Y.; Krishnamurthi, K.; Mudliar, S. N.; Yadav, R. R.; Fulke, A. B.; Devi, S. S.; Chakrabarti, T., Recent Advancements in Carbonic Anhydrase–Driven Processes for $CO_2$ Sequestration: Minireview. *Crit. Rev. Environ. Sci. Technol.* **2012,** *42*, 1419-1440.
5. Arazawa, D. T.; Oh, H. I.; Ye, S. H.; Johnson, C. A., Jr.; Woolley, J. R.; Wagner, W. R.; Federspiel, W. J., Immobilized Carbonic Anhydrase on Hollow Fiber Membranes Accelerates $CO_2$ Removal from Blood. *J. Membr. Sci.* **2012,** *404*, 25-31.
6. Zhang, Y.-T.; Zhang, L.; Chen, H.-L.; Zhang, H.-M., Selective Separation of Low Concentration $CO_2$ using Hydrogel Immobilized CA Enzyme Based Hollow Fiber Membrane Reactors. *Chem. Eng. Sci.* **2010,** *65*, 3199-3207.
7. Zhang, S.; Zhang, Z.; Lu, Y.; Rostam-Abadi, M.; Jones, A., Activity and Stability of Immobilized Carbonic Anhydrase for Promoting $CO_2$ Absorption into a Carbonate Solution for Post-Combustion $CO_2$ Capture. *Bioresour. Technol.* **2011,** *102*, 10194-201.
8. Vinoba, M.; Bhagiyalakshmi, M.; Jeong, S. K.; Yoon, Y. I.; Nam, S. C., Immobilization of Carbonic Anhydrase on Spherical SBA-15 for Hydration and Sequestration of $CO_2$. *Colloid Surface B* **2012,** *90*, 91-96.
9. Vinoba, M.; Lim, K. S.; Lee, S. H.; Jeong, S. K.; Alagar, M., Immobilization of Human Carbonic Anhydrase on Gold Nanoparticles Assembled onto Amine/Thiol-Functionalized Mesoporous SBA-15 for Biomimetic Sequestration of $CO_2$. *Langmuir* **2011,** *27*, 6227-6234.
10. Ozdemir, E., Biomimetic $CO_2$ Sequestration: 1. Immobilization of Carbonic Anhydrase within Polyurethane Foam. *Energ. Fuel* **2009,** *23*, 5725-5730.
11. Gabelman, A.; Hwang, S.-T., Hollow Fiber Membrane Contactors. *J. Membr. Sci.* **1999,** *159*, 61-106.
12. Li, S.; Rocha, D. J.; James Zhou, S.; Meyer, H. S.; Bikson, B.; Ding, Y., Post-Combustion $CO_2$ Capture Using Super-Hydrophobic, Polyether Ether Ketone, Hollow Fiber Membrane Contactors. *J. Membr. Sci.* **2013,** *430*, 79-86.
13. Wilcox, J., *Carbon Capture*. Springer: New York, 2012.
14. Larachi, F.; Lacroix, O.; Grandjean, B. P. A., $CO_2$ Hydration by Immobilized Carbonic Anhydrase in Robinson–Mahoney and Packed-Bed Scrubbers—Role of Mass Transfer and Inhibitor Removal. *Chem. Eng. Sci.* **2012,** *73*, 99-115.
15. Decher, G., Fuzzy Nanoassemblies: Toward Layered Polymeric Multicomposites. *Science* **1997,** *277*, 1232-1237.
16. Caruso, F.; Caruso, R. A.; Möhwald, H., Nanoengineering of Inorganic and Hybrid Hollow Spheres by Colloidal Templating. *Science* **1998,** *282*, 1111-1114.
17. Caruso, F.; Niikura, K.; Furlong, D. N.; Okahata, Y., 2. Assembly of Alternating Polyelectrolyte and Protein Multilayer Films for Immunosensing. *Langmuir* **1997,** *13*, 3427-3433.
18. Onda, M.; Lvov, Y.; Ariga, K.; Kunitake, T., Sequential Reaction and Product Separation on Molecular Films of Glucoamylase and Glucose Oxidase Assembled on an Ultrafilter. *J. Ferment. Bioeng.* **1996,** *82*, 502-506.

19. Yu, A.; Liang, Z.; Caruso, F., Enzyme Multilayer-Modified Porous Membranes as Biocatalysts. *Chem. Mater.* **2005,** *17*, 171-175.
20. Lvov, Y.; Ariga, K.; Ichinose, I.; Kunitake, T., Assembly of Multicomponent Protein Films by Means of Electrostatic Layer-by-Layer Adsorption. *J. Am. Chem. Soc.* **1995,** *117*, 6117-6123.
21. Ichinose, I.; Kuroiwa, K.; Lvov, Y.; Kunitake, T., Recent Progress in the Surface Sol-Gel Process and Protein Multilayers. In *Multilayer Thin Films*, Decher, G.; Schlenoff, J. B., Eds. Wiley-VCH: Weinheim, 2003; pp 155-175.
22. Asuri, P.; Karajanagi, S. S.; Vertegel, A. A.; Dordick, J. S.; Kane, R. S., Enhanced Stability of Enzymes Adsorbed onto Nanoparticles. *J. Nanosci. Nanotechnol.* **2007,** *7*, 1675-1678.
23. Hou, J.; Dong, G.; Ye, Y.; Chen, V., Laccase Immobilization on Titania Nanoparticles and Titania-Functionalized Membranes. *J. Membr. Sci.* **2014,** *452*, 229-240.
24. Zhang, S.; Lu, Y.; Ye, X., Catalytic Behavior of Carbonic Anhydrase Enzyme Immobilized onto Nonporous Silica Nanoparticles for Enhancing $CO_2$ Absorption into a Carbonate Solution. *Int. J. Greenh. Gas Con.* **2013,** *13*, 17-25.
25. Wang, Y.; Caruso, F., Mesoporous Silica Spheres as Supports for Enzyme Immobilization and Encapsulation. *Chem. Mater.* **2005,** *17*, 953-961.
26. Penders-van Elk, N. J. M. C.; Hamborg, E. S.; Huttenhuis, P. J. G.; Fradette, S.; Carley, J. A.; Versteeg, G. F., Kinetics of Absorption of Carbon Dioxide in Aqueous Amine and Carbonate Solutions with Carbonic Anhydrase. *Int. J. Greenh. Gas Con.* **2013,** *12*, 259-268.
27. Onda, M.; Ariga, K.; Kunitake, T., Activity and Stability of Glucose Oxidase in Molecular Films Assembled Alternately with Polyions. *J. Biosci. Bioeng.* **1999,** *87*, 69-75.
28. Zhang, K.; Xu, L. L.; Jiang, J. G.; Calin, N.; Lam, K. F.; Zhang, S. J.; Wu, H. H.; Wu, G. D.; Albela, B.; Bonneviot, L.; Wu, P., Facile Large-Scale Synthesis of Monodisperse Mesoporous Silica Nanospheres with Tunable Pore Structure. *J. Am. Chem. Soc.* **2013,** *135*, 2427-2430.
29. Caruso, F.; Niikura, K.; Furlong, D. N.; Okahata, Y., 1. Ultrathin Multilayer Polyelectrolyte Films on Gold: Construction and Thickness Determination. *Langmuir* **1997,** *13*, 3422-3426.
30. Olsson, A. L. J.; Quevedo, I. R.; He, D.; Basnet, M.; Tufenkji, N., Using the Quartz Crystal Microbalance with Dissipation Monitoring to Evaluate the Size of Nanoparticles Deposited on Surfaces. *ACS Nano* **2013,** *7*, 7833-7843.
31. Bond, G. M.; Stringer, J.; Brandvold, D. K.; Simsek, F. A.; Medina, M.-G.; Egeland, G., Development of Integrated System for Biomimetic $CO_2$ Sequestration Using the Enzyme Carbonic Anhydrase. *Energ. Fuel* **2001,** *15*, 309-316.
32. Garg, L. C., Catalytic Activity and Inhibition of Carbonic Anhydrase of Rat Tissues. *Biochem. Pharmacol.* **1974,** *23*, 3153-3161.
33. IsoPrime IEF Purification Unit User Manual. https://www.gelifesciences.com/gehcls_images/GELS/Related%20Content/Files/1314729545976/litdocIsoPRIMEum_20110830211647.pdf (accessed 8 July).
34. Lvov, Y.; Ariga, K.; Ichinose, I.; Kunitake, T., Molecular Film Assembly via Layer-by-Layer Adsorption of Oppositely Charged Macromolecules (Linear Polymer, Protein and Clay) and Concanavalin A and Glycogen. *Thin Solid Films* **1996,** *284-285*, 797-801.
35. Crumbliss, A. L.; McLachlan, K. L.; O'Daly, J. P.; Henkens, R. W., Preparation and Activity of Carbonic Anhydrase Immobilized on Porous Silica Beads and Graphite Rods. *Biotechnol. Bioeng.* **1988,** *31*, 796-801.
36. Thee, H.; Smith, K. H.; da Silva, G.; Kentish, S. E.; Stevens, G. W., Carbonic Anhydrase Promoted Absorption of $CO_2$ into Potassium Carbonate Solutions. *Greenh. Gas Sci. Technol.* **2015,** *5*, 108-114.

37. Borchert, M.; Saunders, P., Heat-Stable Carbonic Anhydrases and Their Use. US Patent 20130203156: 2013.
38. Lindskog, S., Structure and Mechanism of Carbonic Anhydrase. *Pharmacol. Ther.* **1997,** *74*, 1-20.
39. Vertegel, A. A.; Siegel, R. W.; Dordick, J. S., Silica Nanoparticle Size Influences the Structure and Enzymatic Activity of Adsorbed Lysozyme. *Langmuir* **2004,** *20*, 6800-6807.
40. Franco, J. A.; Montigny, D. D.; Kentish, S. E.; Perera, J. M.; Stevens, G. W., Effect of Amine Degradation Products on the Membrane Gas Absorption Process. *Chem. Eng. Sci.* **2009**, *64*, 4016-4023.
41. Hoff, K.; Juliussen, O.; Falk-Pedersen, O.; Svendsen, H. F., Modeling and Experimental Study of Carbon Dioxide Absorption in Aqueous Alkanolamine Solutions Using a Membrane Contactor. *Ind. Eng. Chem. Res.* **2004**, *43*, 4908-4921.
42. Capannelli, G.; Comite, A.; Costa, C.; di Felice, R. Effect of Absorbent Type and Concentration on $CO_2$ Capture from a Gas Stream into a Liquid Phase. *Ind. Eng. Chem. Res.* **2013**, *52*, 13128-13136.
43. Decher, G.; Schmitt, J., Fine-Tuning of the Film Thickness of Ultrathin Multilayer Films Composed of Consecutively Alternating Layers of Anionic and Cationic Polyelectrolytes *Progr. Colloid Polym. Sci.* **1992,** *89*, 160-164.
44. Malaisamy, R.; Bruening, M. L., High-Flux Nanofiltration Membranes Prepared by Adsorption of Multilayer Polyelectrolyte Membranes on Polymeric Supports. *Langmuir* **2005,** *21*, 10587-10592.
45. Franco, J. A.; deMontigny, D. D.; Kentish, S. E.; Perera, J. M.; Stevens, G. W., Polytetrafluoroethylene (PTFE)-Sputtered Polypropylene Membranes for Carbon Dioxide Separation in Membrane Gas Absorption: Hollow Fiber Configuration. *Ind. Eng. Chem. Res.* **2012,** *51*, 1376-1382.
46. Franken, A. C. M.; Nolten, J. A. M.; Mulder, M. H. V.; Bargeman, D.; Smolders, C. A., Wetting Criteria for the Applicability of Membrane Distillation. *J. Membr. Sci.* **1987,** *33*, 315-328.
47. García-Payo, M. C.; Izquierdo-Gil, M. A.; Fernández-Pineda, C., Wetting Study of Hydrophobic Membranes via Liquid Entry Pressure Measurements with Aqueous Alcohol Solutions. *J. Colloid Interf. Sci.* **2000,** *230*, 420-431